Weyl disks

Theoretical prediction

Erdmanis, Janis; Lukács, Árpád; Nazarov, Yuli V.

DOI
10.1103/PhysRevB.98.241105

Publication date
2018

Document Version
Final published version

Published in
Physical Review B

Rapid Communications

Weyl disks: Theoretical prediction

Janis Erdmanis, Árpád Lukács, and Yuli V. Nazarov
Department of Quantum Nanoscience, Kavli Institute of Nanoscience, TU Delft, Lorentzweg 1, 2628CJ Delft, The Netherlands

(Received 9 May 2018; revised manuscript received 2 October 2018; published 5 December 2018)

A variety of quantum systems exhibit Weyl points in their spectra where two bands cross in a point of three-dimensional parameter space with conical dispersion in the vicinity of the point. We consider theoretically the soft constraint regime where the parameters are dynamical quantum variables. We have shown that in general the soft constraints, in the quasiclassical limit, result in Weyl disks where two states are (almost) degenerate in a finite two-dimensional region of the three-dimensional parameter space. We provide concrete calculations for two setups: Weyl point in a four-terminal superconducting structure and a Weyl exciton, i.e., a bound state of Weyl electron and a massive hole.

DOI: 10.1103/PhysRevB.98.241105

The Weyl equation is written to describe the propagation of massless fermions [1,2]. The 2×2 Weyl Hamiltonian is linear in the particle momenta $\mathbf{k}$ and has a conical spectrum with degeneracy at $\mathbf{k} = 0$. The Weyl equation describes neutrini if their masses can be neglected [3].

A variety of quantum systems exhibit similar spectral singularities in the vicinity of crossing of two bands in three-dimensional (3D) parameter space. The degeneracy points are referred to as Weyl points (WP). In solid-state physics, the parameter space is the Brillouin zone of a crystal lattice and Weyl physics is an active subject in experimental and theoretical research. WP are predicted theoretically in Refs. [4–6] and have been recently observed experimentally [7,8]. For reviews on materials hosting WPs, see Refs. [9,10]. In the case of polyatomic molecules, the parameter space for Born-Oppenheimer energy levels is the positions of the nuclei; the existence of points of degeneracy is demonstrated in Refs. [11–13]. For molecular nanomagnets, the parameter space is the direction and magnitude of the external magnetic field; WPs result in resonances in tunneling probability [14,15]. In the context of quantum transport, a setup with a WP in the space of two gate voltages and a superconducting phases has been proposed to realize a robust quantized current source [16]. WPs have been recently predicted [17,18] in the spectrum of Andreev bound states (ABS) [19] in four terminal superconducting nanostructures where three independent phases form 3D parameter space. Quantized topological transconductance has been predicted. Similarly, WP can be also realized in three terminal nanostructures [20] and other systems [21,22].

It seems a relevant approximation to treat the parameters forming the space where the WP occurs as fixed numbers (hard constraint). However, a much more realistic and general situation is where the parameters are dynamical quantum variables, which can be the subject of fluctuations and also backaction from the system hosting the WP. To describe this situation of a *soft constraint*, one would, e.g., promote a parameter x to an operator $\hat{x}$, add an energy term $A(\hat{x} - x_0)^2$ that attempts to constrain $\hat{x}$ to x_0 at sufficiently large A, and add a Hamiltonian accounting for the dynamics of $\hat{x}$.

In this Rapid Communication, we demonstrate the drastic consequences of a soft constraint in the vicinity of a WP. The degeneracy of two bands that has been restricted to a singular point for a hard constraint, in the quasiclassical limit spreads over to a finite two-dimensional region that we term *Weyl disk*. Quantum effects lift the degeneracy at the disk, resulting in strong anisotropy of the conical spectrum. We assess the situation in detail and provide detailed calculation of the quantum spectrum for two very different and physically interesting setups. The first setup is a multiterminal superconducting nanostructure embedded in a linear circuit. The second setup is an exemplary band structure where a *Weyl exciton* consisting of a Weyl electron and a massive hole can be formed.

Let us shortly stress the relevance of the setup and the concrete significance of our results; more details are given in Ref. [23]. The superconducting nanonstructures (with WPs) can be easily fabricated and implemented as nanodevices, and quantum manipulation in similar devices has been experimentally verified [24]. The Weyl disk regime described provides extra opportunities for quantum computing owing to the degeneracy of the quantum states, such degeneracies have been the basis of holonomic [25,26] and topological quantum computing [27–29]. We find practical candidates for Weyl excitons in materials such as graphene, germanene, TaAs, TaP, and NbAs. We predict a unique property of Weyl excitons: In the Weyl disk regime, they can only move in one direction. This can be observed in a simple experiment we describe [23].

Let us describe the setups in detail. As shown in Ref. [17], the ABS spectrum of a four-terminal superconducting nanostructure can have WPs where ABS energy reaches zero (relative to Fermi level). This implies that the ground state of the nanostructure is close to the first excited singlet state. We count the phases from the WP position. The effective Hamiltonian in the vicinity of the WP reads $\hat{H}_{\mathrm{WP}} = (\hbar/2e) I_{na} \hat{\phi}_n \hat{\sigma}_a$, where $\hat{\sigma}_a$ denote the Pauli matrices in the space of ground and excited singlet states [17]. The soft constraint situation occurs naturally if one takes into account self-inductances of the superconducting leads and associated capacitances (see Fig. 1). This promotes the superconducting phases at the nanostructure to dynamical variables $\hat{\phi}_n$, which are softly constrained to the superconducting phases ϕ_n^r, fixed by the magnetic fluxes in the corresponding superconducting loops.

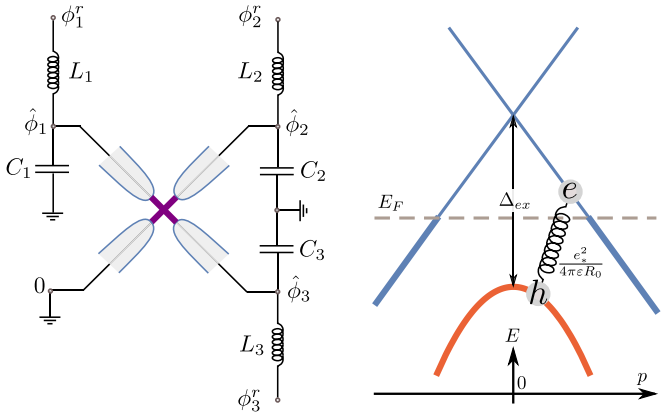

FIG. 1. The two setups under consideration. Left: the four-terminal superconducting nanostructure embedded in a linear circuit made of small inductances $L_{1,2,3}$ and capacitances $C_{1,2,3}$. Right: a model band structure that supports Weyl excitons with energy $\approx\Delta_{ex}$ that are bound states of a Weyl electron and a massive hole, with the hole mass providing a soft constraint for the electron momentum.

The full Hamiltonian encompasses inductive and capacitive energy and reads [17,30,31]

$$\hat{H} = \hat{H}_{\rm WP} + \sum_n \left[\frac{(\hbar/2e)^2}{2L_n} \left(\hat{\phi}_n - \phi_n^r\right)^2 + \frac{(2e\hat{N}_n)^2}{2C_n} \right]. \quad (1)$$

Here the number operators $\hat{N}_n$ are canonically conjugate variables to the phases $\hat{\phi}_n$: $[\hat{N}_n, \hat{\phi}_m] = -i\delta_{nm}$ [19]. Here the inductive energy provides the soft constraint, and the capacitive energy is responsible for the quantum fluctuations of the phases.

For a complementary example with very different physical content, let us consider a solid exemplary band structure [Fig. 1(b)]. It comprises an electron band with a WP and a parabolic valence band. To soft constrain the momentum of the Weyl electron, let us tie it to a massive hole coming from the valence band. The bond is naturally provided by the Coulomb interaction and the resulting particle is a sort of exciton, described by the Hamiltonian

$$\hat{H}_{\rm ex} = \Delta_{\rm ex} + \hat{H}_{\rm WP} + \sum_n \frac{\left(\hat{p}_n - p_n^T\right)^2}{2m_n^*} - \frac{e_*^2}{4\pi\epsilon_0 r}, \quad (2)$$

where we count all momenta from the quasimomentum of the Weyl point, $\hat{H}_{\rm WP} = v_{na}\hat{p}_n\hat{\sigma}_a$, $\hat{p}_n$ are the components of the quasimomentum of the Weyl electron, p_n^T are those of the total exciton quasimomentum, m_n^* are the (possibly anisotropic) hole masses, and the last term presents Coulomb attraction between electron and hole, with $r = |\mathbf{r}|$ being the distance between these two particles.

Let us note the close similarity: $H_{\rm WP}$ and the soft constraint term in Eq. (2) are brought to the form in Eq. (1) with the replacements $p_n \to P\phi_n$, $Pv_{na} \to (\hbar/2e)I_{na}$, $(P^2/2m_n^*) \to (\hbar/2e)^2/2L_n$, where P is a constant with momentum dimension. Since $\mathbf{r}$ is canonically conjugate to $\mathbf{p}$, the Coulomb energy plays a role similar to the capacitive energy in the Hamiltonian (1), providing the quantum fluctuations of $\mathbf{p}$.

For both setups, we evaluate the energies of the discrete quantum states, analyzing their dependence on the parameters, either ϕ_n^r or p_n^T.

Systems described by the Hamiltonians (1) and (2), depending on the parameters, can be in two regimes: the quasiclassical and the opposite, deeply quantum one.

To understand the regimes, let us consider the one-dimensional version of Eq. (1). It is exactly solvable, since the quasispin part has a single spin component, which can be diagonalized simultaneously with the Hamiltonian. For the spin eigenvalue $\sigma = \pm 1$, the kinetic part of the Hamiltonian is $(\hbar/2e)^2(1/2L)(\hat{\phi} - \phi^r + \sigma\phi_0)^2 - LI^2/2$, with $\phi_0 = (2e/\hbar)IL$. At $\phi^r = 0$, it gives rise to two degenerate minima separated by $2\phi_0$ with an energy barrier $E_B = LI^2/2$ between them. The Hamiltonian for both values of σ is that of a harmonic oscillator, with frequency $\omega = 1/\sqrt{LC}$. The quasiclassical parameter $\mathcal{Q}$ is defined as the ratio of the barrier height and the energy quantization of the oscillators, and reads

$$\mathcal{Q} = \frac{1}{2}\left(\frac{LIe}{\hbar}\right)^2 \frac{\hbar}{e^2 Z}, \quad (3)$$

where $Z = \sqrt{L/C}$ is the characteristic impedance of the oscillator. In Eq. (3), an estimation for the first term is ratio of the inductance of the circuit to the typical inductance of the nanostructure, which has to be small to provide good confinement. However, the second term is large, estimated as the ratio of vacuum impedance to resistance quantum $\sim 10^2$. This is why the quasiclassical limit $\mathcal{Q} \gg 1$ is well achievable (see detailed estimations in Ref. [23]). In a 3D case, we define $\mathcal{Q}$ with respect to the maximal $L_n I_n^2$ (*easy direction*).

Similar analysis for the Hamiltonian (2) yields in one dimension (1D) a barrier height of $E_B = m^* v^2/2$. The parameter $\mathcal{Q}$ is defined as the ratio of the barrier height to the ground-state Coulomb binding energy $E_b \propto (e_*^2/4\pi\epsilon_0)^2 m^*/2\hbar^2$, yielding

$$\mathcal{Q} = \left(\frac{\hbar v 4\pi\epsilon_0}{e_*^2}\right)^2. \quad (4)$$

If one estimates the Weyl velocity v with the typical Fermi velocity for metals $v_F \sim 10^6 \mathrm{ms}^{-1}$, and the dielectric constant as $\epsilon_r \approx 10$, $\mathcal{Q} \sim 25$, the quasiclassical limit is well achievable in solids. In a 3D case, we define $\mathcal{Q}$ with the parameters in the easy direction (maximal mv^2).

The deeply quantum limit $\mathcal{Q} \ll 1$ is in fact not interesting, since there the Weyl energy is not modified by the soft constraint, except for trivial perturbative corrections.

In this study, we concentrate on the quasiclassical limit. We give analytical results valid at $\mathcal{Q} \gg 1$ and numerical results for $\mathcal{Q} \sim 5$.

In the quasiclassical regime, we neglect the fluctuations of the phases ϕ_n and replace the quasispin term $H_{\rm WP}$ with one of its eigenvalues. The matrix I_{na} can be diagonalized by a coordinate transformation $I_{na} \to I_n\delta_{na}$ [23]. Then we need to minimize

$$E_{{\rm cl},\sigma} = \frac{\sigma\hbar}{2e}\sqrt{\sum_n I_n^2\phi_n^2} + \left(\frac{\hbar}{2e}\right)^2 \sum_n \frac{\left(\phi_n - \phi_n^r\right)^2}{2L_n}. \quad (5)$$

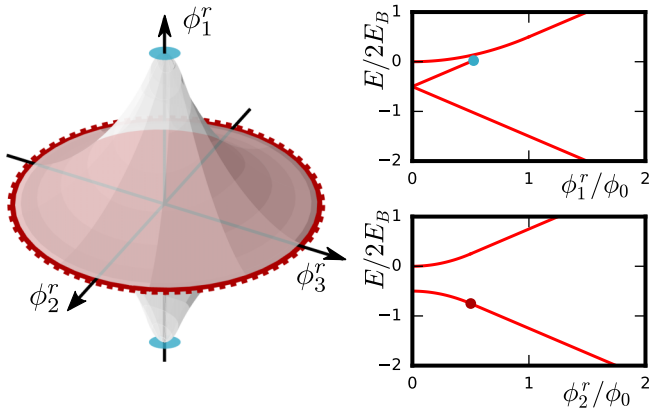

FIG. 2. The Weyl disk. Left: The region in parameter space ϕ_n^r (or p_n^T) where three quasiclassical energy minima exists. The two minima are degenerate at the disk in the plane (ϕ_2^r, ϕ_3^r). Right: The quasiclassical energy spectrum in the easy direction (top) and in a direction within the disk (bottom). The dots mark the region edges. (The parameter choice is $L_n = L/n$ and $I_n = I$.)

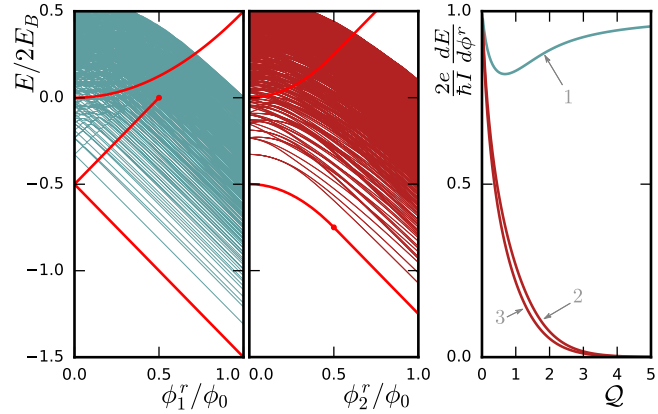

FIG. 3. The energy spectrum of the circuit shown in Fig. 1 for $\mathcal{Q} = 5$ in the easy direction (left panel) and in the plane of the disk (center panel). The parameters are $L_n = L/n$, $C_n = C = \hbar^2\mathcal{Q}^2/LE_B^2$, $I_n = I$, and $\mathcal{Q} = 5$ (L and I arbitrary). We also show the "velocities" $\partial E/\partial\phi_n^r$ versus the quasiclassical parameter $\mathcal{Q}$ in the ground state (right panel).

If $|\phi_n^r| \gg \phi_0$, the minimization reproduces the two cones of the Weyl spectrum, $(\sigma\hbar/2e)\sqrt{\sum_n I_n^2(\phi_n^r)^2}$. In the vicinity of the Weyl point $|\phi_n| \sim \phi_0$, the Weyl spectrum is drastically modified (see Fig. 2). Most important, the minimization gives two minima for $\sigma = -1$ in the 3D region shown in the figure. These two minima are precisely degenerate at a 2D *Weyl disk*, which is perpendicular to the easy direction, where $L_n I_n^2$ is maximal ($n = 1$ for the easy direction). The disk is an ellipse with dimensions $(4e/\hbar)(L_1 I_1^2 - L_m I_m^2)/I_m$, $m = 2, 3$.

In Fig. 2, we plot the energies along the easy direction and in the plane of the disk. There is a linear dependence of the energies in the easy direction. The second minimum for $\sigma = -1$ disappears at a critical value of ϕ_1^r. For even larger ϕ_1^r, the Weyl spectrum $E \approx (\hbar/2e)I_1\sigma\phi_1^r$ is seen again. If we move along the disk, two minima remain degenerate until they merge at the disk edge.

The same minimization applies to the Weyl exciton setup. In this case, the lowest curves in Fig. 2 define the lower boundary of the continuous spectrum. The bound exciton states follow the edge at slightly lower energy, with binding energy $E_b \ll E_B$. If we move along the disk, all bound states remain doubly degenerate, until the edge of the disk. They split linearly if we move in the easy direction.

This brings us to the main conclusion of the paper: In the quasiclassical limit $\mathcal{Q} \gg 1$, soft constraints extend the isolated degeneracy in the WP into a finite 2D region. This property of WP can be used for the purposes of quantum manipulation and computation.

At large but finite values of $\mathcal{Q}$, the degeneracy at the disk is lifted, albeit the corresponding energy splittings remain relatively small at moderate values of $\mathcal{Q}$. We illustrate this with numerical results for both setups. In Fig. 3, we plot the full energy spectrum of the superconducting nanostructure for $\mathcal{Q} = 5$. Besides the ground state, the spectrum includes the corresponding excitations in three oscillators. For comparison, in Fig. 3, we plot in red the quasiclassical results from Fig. 2. Upon a small shift, the lowest curves give good approximations for the numerical energies of the lowest states.

At $\phi^r = 0$, all levels are doubly degenerate. If we move in the easy direction, the levels are split with $\Delta E \propto (\hbar/e)I_1\phi_1^r$. The levels become increasingly dense at higher energies. Since the levels begin to cross, this behavior is restricted to increasingly small values of ϕ_1^r. At $\phi_1^r < 0.5\phi_0$, the crossings are avoided at an exponentially small energy scale corresponding to the tunneling amplitude between the minima. The amplitude increases with energy owing to a bigger overlap of the oscillator excited states in two minima.

If we move in a perpendicular direction, we observe an exponentially small energy splitting at $\phi_{2,3} \approx 0.4\phi_0$. At small $\phi_{2,3}^r$, the splitting is $\Delta E \approx (\hbar/e)I_{2,3}\phi_{2,3}^r e^{-2\mathcal{Q}}$ in the ground state [23]. We see this suppression in the plot of the normalized "velocities" of the lowest state, $(2e/\hbar I_1)\partial E/\partial\phi_n^r$ at $\phi^r \to 0$ (Fig. 3, right panel). In the deep quantum limit, $\mathcal{Q} \lesssim 1$, all velocities remain the same as for the original Weyl spectrum. The velocity in the easy direction stays closer to this value at any $\mathcal{Q}$.

In Fig. 4, we show the spectrum of the exciton Hamiltonian (2) for $\mathcal{Q} = 20$. For the sake of numerical efficiency, we have computed the spectrum in the 2D limit. This is valid in the highly anisotropic limit $m_3^* \ll m_{1,2}^*$. Also, graphene provides a practical example of a stable conical spectrum in 2D. With graphene data, $v \approx v_F$ and a substrate with a relative permittivity $\sim$10, $\mathcal{Q} \sim 20$ [32]. The continuous spectrum is shown by the shaded region. Its lower edge is given by the quasiclassical result (Fig. 2). Below the edge, we plot the energies of the five lowest bound states. If we go in the easy direction, we observe an almost unmodified Weyl spectrum for the lowest and the first excited states. In contrast to this, the splitting between these states remains small in the plane of the disk. This is seen for the lowest and the first excited states as for third and fourth excited states that are close to the edge. In the right panel of Fig. 4, we plot the normalized velocities of the lowest state versus $\mathcal{Q}$. Similarly to the case of the superconducting nanostructure, the Weyl velocity in the easy direction is hardly modified, while that in perpendicular direction is strongly suppressed with increasing $\mathcal{Q}$. In fact,

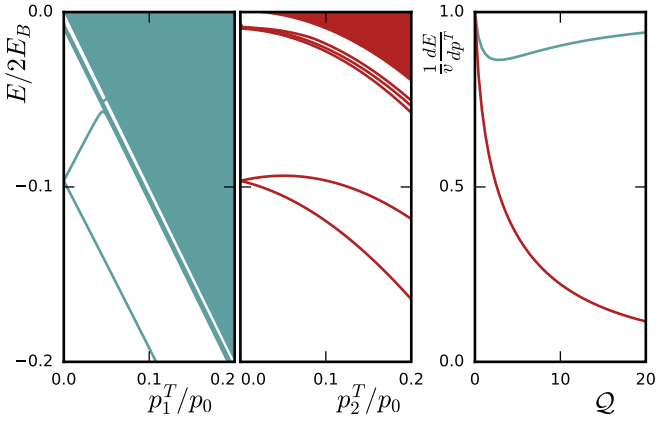

FIG. 4. The energy spectrum of a two-dimensional anisotropic Weyl exciton for $\mathcal{Q} = 20$ in the easy direction (left panel) and in the plane of the disk (center panel). The parameters are $m_n = m/n$, $v_n = v$, $e_*^2 = \hbar v 4\pi\epsilon_0/\sqrt{\mathcal{Q}}$, and $\mathcal{Q} = 20$ (v and m arbitrary). We also show the velocities $\partial E/\partial p_n^T$ versus the quasiclassical parameter $\mathcal{Q}$ in the lowest state of the exciton (right panel).

the wave function of the bound state near one of the minima is singular in coordinate space owing to the the singularity of the Coulomb potential at $r \to 0$. The calculation of the amplitude of tunneling between the minima demonstrates that the value of the amplitude is determined by this singularity. This results in power-law suppression $\partial E/\partial p_n^T = \pm v_n/2\mathcal{Q}^4$ in the ground state [23] in 3D. In 2D, $\partial E/\partial p_n^T = \pm v_n/2(\mathcal{Q}/4)^3$. [In 2D, we use the definition $\mathcal{Q} = 4E_B/E_b$ to obtain Eq. (4).]

In conclusion, we have shown that a Weyl spectrum is essentially modified by soft constraints of the spectral parameters in the quasiclassical limit. A Weyl disk emerges in the vicinity of the WP. There are two degenerate states at the disk, that are slightly split at moderate values of the quasi-classical parameter $\mathcal{Q}$.

We illustrate this general statement with two examples of very different physical systems. The first system is a multiterminal superconducting nanostructure where the spectral parameters are the superconducting phases and the soft constraint is realized by an external circuit. The second example concerns a Weyl exciton that is the bound state of a Weyl electron and a massive hole. The mass provides a soft constraint of the total exciton quasimomentum to the momentum of the Weyl electron. We show that in both examples, the quasiclassical regime can be achieved with a reasonable parameter choice.

This project has received funding from the European Research Council (ERC) under the European Union's Horizon 2020 research and innovation programme (Grant Agreement No. 694272).

[1] H. Weyl, Z. Phys. **56**, 330 (1929).
[2] P. B. Pal, Am. J. Phys. **79**, 485 (2011).
[3] T.-P. Cheng and L.-F. Li, *Gauge Theory of Elementary Particle Physics* (Clarendon Press, Oxford, UK, 1984).
[4] C. Herring, Phys. Rev. **52**, 365 (1937).
[5] S.-M. Huang, S.-Y. Xu, I. Belopolski, C.-C. Lee, G. Chang, B. Wang, N. Alidoust, G. Bian, M. Neupane, C. Zhang *et al.*, Nat. Commun. **6**, 7373 (2015).
[6] S. Murakami, New J. Phys. **9**, 356 (2007).
[7] L. Lu, Z. Wang, D. Ye, L. Ran, J. D. Joannopoulos, and M. Soljacic, Science **349**, 622 (2015).
[8] S.-Y. Xu, I. Belopolski, N. Alidoust, M. Neupane, G. Bian, C. Zhang, R. Sankar, G. Chang, Z. Yuan, C.-C. Lee *et al.*, Science **349**, 613 (2015).
[9] M. Z. Hasan and C. L. Kane, Rev. Mod. Phys. **82**, 3045 (2010).
[10] B. Yan and C. Felser, Annu. Rev. Condensed Matter Phys. **8**, 337 (2017).
[11] G. Herzberg and H. C. Longuet-Higgins, Discuss. Faraday Soc. **35**, 77 (1963).
[12] F. Faure and B. I. Zhilinskii, Phys. Rev. Lett. **85**, 960 (2000).
[13] B. I. Zhilinskii, Phys. Rep. **341**, 85 (2001).
[14] W. Wernsdorfer and R. Sessoli, Science **284**, 133 (1999).
[15] W. Wernsdorfer, N. E. Chakov, and G. G. Christou, Phys. Rev. Lett. **95**, 037203 (2005).
[16] R. Leone, L. P. Lévy, and P. Lafarge, Phys. Rev. Lett. **100**, 117001 (2008).
[17] R.-P. Riwar, M. Houzet, J. S. Meyer, and Y. V. Nazarov, Nat. Commun. **7**, 11167 (2016).
[18] E. Eriksson, R.-P. Riwar, M. Houzet, J. S. Meyer, and Y. V. Nazarov, Phys. Rev. B **95**, 075417 (2017).
[19] Y. V. Nazarov and Y. M. Blanter, *Quantum Transport* (Cambridge University Press, Cambridge, UK, 2009).
[20] J. S. Meyer and M. Houzet, Phys. Rev. Lett. **119**, 136807 (2017).
[21] S. A. Yang, H. Pan, and F. Zhang, Phys. Rev. Lett. **113**, 046401 (2014).
[22] F. Zhang and C. L. Kane, Phys. Rev. B **90**, 020501(R) (2014).
[23] See Supplemental Material at http://link.aps.org/supplemental/10.1103/PhysRevB.98.241105 for additional information on possible applications in quantum computing, prediction of exciton data, a proposed experiment, and details for the calculations, which includes Refs. [33–44].
[24] C. Janvier, L. Tosi, L. Bretheau, Ç. Girit, M. Stern, P. Bertet, P. Joyez, D. Vion, D. Esteve, M. F. Goffman *et al.*, Science **349**, 1199 (2015).
[25] P. Zanardi and M. Rasetti, Phys. Lett. A **264**, 94 (1999).
[26] J. Pachos, P. Zanardi, and M. Rasetti, Phys. Rev. A **61**, 010305 (1999).
[27] M. H. Freedman, A. Kitaev, M. J. Larsen, and Z. Wang Bull. Am. Math. Soc. **40**, 31 (2003).
[28] E. Sjöqvist, Physics **1**, 35 (2008).
[29] V. Lahtinen and J. Pachos, SciPost Physics **3**, 021 (2017).
[30] D. V. Averin and K. K. Likharev, J. Low. Temp. Phys. **62**, 345 (1986).
[31] A. I. Larkin, K. K. Likharev, and Yu. N. Ovchinnikov, Phys. B (Amsterdam) **126**, 414 (1984).
[32] A. H. Castro Neto, F. Guinea, N. M. R. Peres, K. S. Novoselov, and A. K. Geim, Rev. Mod. Phys. **81**, 109 (2009).
[33] V. Mourik, K. Zuo, S. M. Frolov, S. R. Plissard, E. P. A. M. Bakkers, and L. P. Kouwenhoven, Science **336**, 1003 (2012).

[34] P. Solinas, P. Zanardi, and N. Zanghì, Phys. Rev. A **70**, 042316 (2004).
[35] P. Miró, M. Audiffred, and T. Heine, Chem. Soc. Rev. **43**, 6537 (2014).
[36] E. Kogan and V. U. Nazarov, Phys. Rev. B **85**, 115418 (2012).
[37] Quantumwise A/S, Band structure of 2d graphene [https://quantumwise.com/documents/tutorials/latest/BasicGrapheneTutorial/index.html/chap.graphene_bandstructure.html].
[38] L. Zhang, P. Bampoulis, A. N. Rudenko, Q. Yao, A. van Houselt, B. Poelsema, M. I. Katsnelson, and H. J. W. Zandvliet, Phys. Rev. Lett. **116**, 256804 (2016).
[39] D. Grassano, O. Pulci, A. M. Conte, and F. Bechstedt, Sci. Rep. **8**, 3534 (2018).
[40] J. Buckeridge, D. Jevdokimovs, C. R. A. Catlow, and A. A. Sokol, Phys. Rev. B **93**, 125205 (2016).
[41] C.-C. Lee, S.-Y. Xu, S.-M. Huang, D. S. Sanchez, I. Belopolski, G. Chang, G. Bian, N. Alidoust, H. Zheng, M. Neupane *et al.*, Phys. Rev. B **92**, 235104 (2015).
[42] R. S. Knox, *Theory of Excitons* (Academic Press, New York, 1963).
[43] R. Loudon, Proc. Phys. Soc. London **80**, 952 (1962).
[44] J. Erdmanis, Á. Lukács, and Y. Nazarov, 10.5281/zenodo.1433886, See for code used for the numerical calculations.